Inorg. Chem. **2006**, *45*, 8887–8894

Experimental and Theoretical Evaluation of the Charge Distribution over the Ruthenium and Dioxolene Framework of [Ru(OAc)(dioxolene)(terpy)] (terpy = 2,2′:6′,2″-terpyridine) Depending on the Substituents

Tohru Wada,[†] Masahiro Yamanaka,[‡] Tetsuaki Fujihara,[†] Yuji Miyazato,[†] and Koji Tanaka*,[†]

Institute for Molecular Science, CREST, Japan Science and Technology Agency (JST), 5-1 Higashiyama, Myodaiji, Okazaki, Aichi 444-8787, and Department of Chemistry, Rikkyo University, CREST, JST, 3-34-1 Nishi-Ikebukuro, Toshima-Ku, Tokyo 171-8501, Japan

Received April 24, 2006

A series of ruthenium complexes [Ru(OAc)(dioxolene)(terpy)] having various substituents on the dioxolene ligand (dioxolene = 3,5-*t*-$Bu_2C_6H_2O_2$ (**1**), 4-*t*-$BuC_6H_3O_2$ (**2**), 4-$ClC_6H_3O_2$ (**3**), 3,5-$Cl_2C_6H_2O_2$ (**4**), $Cl_4C_6O_2$ (**5**); terpy = 2,2′:6′2″-terpyridine) were prepared. EPR spectra of these complexes in glassy frozen solutions (CH_2Cl_2:MeOH = 95:5, v/v) at 20 K showed anisotropic signals with **g** tensor components 2.242 > g_1 > 2.104, 2.097 > g_2 > 2.042, and 1.951 > g_3 > 1.846. An anisotropic value, $\Delta g = g_1 - g_3$, and an isotropic *g* value, $\langle g \rangle = [(g_1^2 + g_2^2 + g_3^2)/3]^{1/2}$, increase in the order **1** < **2** < **3** < **4** < **5**. The resonance between the Ru^{II}(sq) (sq = semiquinone) and Ru^{III}(cat) (cat = catecholato) frameworks shifts to the latter with an increase of the number of electron-withdrawing substituents on the dioxolene ligand. DFT calculations of **1**, **2**, **3**, and **5** also support the increase of the Ru spin density (Ru^{III} character) with an increase of the number of Cl atoms on the dioxolene ligand. The singly occupied molecular orbitals (SOMOs) of **1** and **5** are very similar to each other and stretch out the Ru–dioxolene frameworks, whereas the lowest unoccupied molecular orbital (LUMO) of **5** is localized on Ru and two oxygen atoms of dioxolene in comparison with that of **1**. Electron-withdrawing groups decrease the energy levels of both the SOMO and LUMO. In other words, an increase in the number of Cl atoms in the dioxolene ligand results in an increase of the positive charge on Ru. Successive shifts in the electronic structure between the Ru^{II}(sq) and Ru^{III}(cat) frameworks caused by the variation of the substituents are compatible with the experimental data.

Introduction

There has been growing interest in transition-metal complexes with "noninnocent" ligands due to their characteristic redox behavior. The term noninnocent is used when the ligands in a complex have strong electrochemical interactions with the central metal.[1] Metal complexes with noninnocent ligands, therefore, are featured by particular combinations of metals and ligands rather than by redox-active ligands alone. Among various metal complexes bearing noninnocent ligands such as dioxolenes, dithiolenes, and benzoquinonediimines,[2] ruthenium−dioxolene complexes are particularly interesting because of their close energy levels between the d-orbital and the π-orbital of the metal and the dioxolene ligand, respectively.[3,4] As a result, there are formally six possible electronic structures for $Ru^{II/III}$−dioxolene complexes (Scheme 1).

A number of Ru^{II} and Ru^{III} complexes with 1,2-benzosemiquinone (sq) and catecholato (cat) ligands have been documented so far, though the actual electronic states of these complexes would lie somewhere between those of two extreme structures. For example, $[Ru^{II}(3,5\text{-}t\text{-}Bu_2q)(bpy)_2]^{2+}$

* To whom correspondence should be addressed. E-mail: ktanaka@ims.ac.jp.
[†] Institute for Molecular Science.
[‡] Rikkyo University.

(1) (a) Jφrgensen, C. K. *Oxidation Numbers and Oxidation States*; Springer: Berlin, 1969; p 213. (b) Ward, M. D.; McCleverty, J. A. *J. Chem. Soc., Dalton Trans.* **2002**, No. 3, 275−288.

(2) (a) Pierpont, C. G.; Buchanan, R. M. *Coord. Chem. Rev.* **1981**, *38* (1), 45−87. (b) Pierpont, C. G.; Lange, C. W. *Prog. Inorg. Chem.* **1994**, *41*, 331−442. (c) Vlcek, A. *Comments Inorg. Chem.* **1994**, *16*, 207−228. (d) Gorelsky, S. I.; Dodsworth, E. S.; Lever, A. B. P.; Vlcek, A. A. *Coord. Chem. Rev.* **1998**, *174*, 469−494. (e) Lever, A. B. P.; Gorelsky, S. I. *Coord. Chem. Rev.* **2000**, *208*, 153−167. (f) Pierpont, C. G. *Coord. Chem. Rev.* **2001**, *216−217*, 99−125. (g) Gorelsky, S. I.; Lever, A. B. P.; Ebadi, M. *Coord. Chem. Rev.* **2002**, *230* (1−2), 97−105. (h) Vlcek, A. *Coord. Chem. Rev.* **2002**, *230* (1−2), 225−242. (i) Lever, A. B. P.; Gorelsky, S. I. *Struct. Bonding (Berlin)* **2004**, *107*, 77.

10.1021/ic060696i CCC: $33.50
Published on Web 10/07/2006

Scheme 1. Redox Series of $Ru^{II/III}$−Dioxolene Complexes

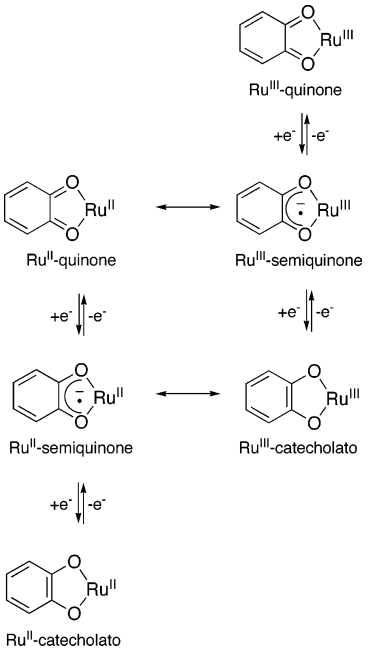

(3,5-*t*-Bu_2q = 3,5-di-*tert*-butylbenzoquinone; bpy = 2,2′-bipyridine) has been assigned as a Ru^{II}(q) complex, though it would more or less involve Ru^{III}(sq) character.[3b,c,e] The unique feature of Ru−dioxolene complexes resulting from strong dπ−pπ interaction also serves to stabilize the unusual electronic structures of Ru complexes, since $[Ru^{III}(OH_2)$(3,5-*t*-Bu_2sq)(terpy)$]^{2+}$ (3,5-*t*-Bu_2sq = 3,5-di-*tert*-butylbenzosemiquinone; terpy = 2,2′:6′,2″-terpyridine) and $[Ru^{III}(OH_2)$(4-Clsq)(terpy)$]^{2+}$ (4-Clsq = 4-chlorobenzosemiquinone) dissociate two and one proton to produce oxyl and hydroxyl radical complexes $[Ru^{II}(O^{\bullet-})$(3,5-*t*-Bu_2sq)(terpy)$]^0$ and $[Ru^{II}$-

Scheme 2. A Series of Ru(OAc) Complexes with Various Dioxolene Ligands

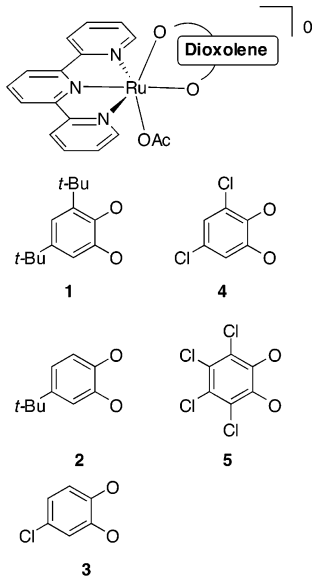

$(O^{\bullet}H)$(4-Clsq)(terpy)$]^+$, respectively.[5] It is, therefore, of high interest to elucidate substituent effects on the charge distribution of the Ru−dioxolene frameworks. In this Article we describe experimental and theoretical studies on the electronic structures of a series of ruthenium complexes [Ru(OAc)-(dioxolene)(terpy)] having various substituents on the dioxolene ligand (Scheme 2).

Experimental Section

Materials. 3,5-Dichlorocatechol (97%) and tetrachlorocatechol (98%) were purchased from Aldrich Chemical Co., Inc. 3,5-Di-*tert*-butylcatechol (>98%), 4-*tert*-butylcatechol (>98%), and 4-chlorocatechol (>98%) were obtained from Tokyo Chemical Industry Co., Ltd. Other agents and solvents were purchased from Wako Pure Chemical Industries, Ltd. and used as supplied.

Syntheses. $RuCl_3$(terpy) was prepared according to the literature.[6] The ruthenium complexes [Ru(OAc)(3,5-*t*-$Bu_2C_6H_2O_2$)(terpy)] (**1**),[5b] [Ru(OAc)(4-$ClC_6H_3O_2$)(terpy)] (**3**),[5b] and [Ru(terpy)($Cl_4C_6O_2$)-(OAc)] (**5**)[4] were synthesized according to previous reports.

[Ru(OAc)(4-*t*-$BuC_6H_3O_2$)(terpy)] (2). This complex was prepared by synthetic procedures similar to those of **1**. A mixture of $RuCl_3$(terpy) (220 mg, 5×10^{-4} mol) and $AgBF_4$ (292 mg, 1.5×10^{-3} mol) in acetone (75 mL) was refluxed for 2 h. After AgCl precipitated out of the solution and was removed by filtration, the filtrate was evaporated to dryness. 4-*tert*-Butylcatechol (84 mg, 5×10^{-4} mol) and methanol (50 mL) were added to the residue, and the mixture was deaerated by bubbling N_2 gas for 30 min. A methanolic solution of AcOK (400 mg in 30 mL) was added to the mixture under N_2, and then the solution was stirred for 2 days under N_2 at room temperature. The resultant purple solution was evaporated to dryness, and the residue was extracted with acetone. The acetone solution was loaded onto a silica gel column (Wakogel C-200, 3 × 15 cm), and the third band eluted with acetone−MeOH (1:1, v/v) was collected. Evaporation of the solvent gave a dark purple powder of **2**. Yield: 159 mg (57%). Anal. Calcd for

(3) (a)Haga, M.; Dodsworth, E. S.; Lever, A. B. P.; Boone, S. R.; Pierpont, C. G. *J. Am. Chem. Soc.* **1986**, *108* (23), 7413−14. (b) Haga, M.; Dodsworth, E. S.; Lever, A. B. P. *Inorg. Chem.* **1986**, *25* (4), 447−53. (c) Boone, S. R.; Pierpont, C. G. *Inorg. Chem.* **1987**, *26* (11), 1769−73. (d) Lever, A. B. P.; Auburn, P. R.; Dodsworth, E. S.; Haga, M. A.; Liu, W.; Melnik, M.; Nevin, W. A. *J. Am. Chem. Soc.* **1988**, *110* (24), 8076−84. (e) Stufkens, D. J.; Snoeck, T. L.; Lever, A. B. P. *Inorg. Chem.* **1988**, *27* (5), 953−6. (f) Ernst, S.; Haenel, P.; Jordanov, J.; Kaim, W.; Kasack, V.; Roth, E. *J. Am. Chem. Soc.* **1989**, *111* (5), 1733−8. (g) Boone, S. R.; Pierpont, C. G. *Polyhedron* **1990**, *9* (18), 2267−72. (h) Bhattacharya, S.; Boone, S. R.; Fox, G. A.; Pierpont, C. G. *J. Am. Chem. Soc.* **1990**, *112* (3), 1088−96. (i) Auburn, P. R.; Dodsworth, E. S.; Haga, M.; Liu, W.; Nevin, W. A.; Lever, A. B. P. *Inorg. Chem.* **1991**, *30* (18), 3502−12. (j) Masui, H.; Lever, A. B. P.; Auburn, P. R. *Inorg. Chem.* **1991**, *30* (10), 2402−10. (k) Bhattacharya, S.; Pierpont, C. G. *Inorg. Chem.* **1991**, *30* (7), 1511−16. (l) Bhattacharya, S.; Pierpont, C. G. *Inorg. Chem.* **1994**, *33* (26), 6038−42. (m) Bhattacharya, S. *Polyhedron* **1994**, *13* (3), 451−6. (n) Ward, M. D. *Inorg. Chem.* **1996**, *35* (6), 1712−14. (o) Santana da Silva, R.; Gorelsky, S. I.; Dodsworth, E. S.; Tfouni, E.; Lever, A. B. P. *Dalton* **2000**, No. 22, 4078−4088.

(4) (a) Tsuge, K.; Tanaka, K. *Chem. Lett.* **1998**, No. 10, 1069−1070. (b) Wada, T.; Tsuge, K.; Tanaka, K. *Angew. Chem., Int. Ed.* **2000**, *39* (8), 1479−1482. (c) Tsuge, K.; Kurihara, M.; Tanaka, K. *Bull. Chem. Soc. Jpn.* **2000**, *73* (3), 607−614. (d) Wada, T.; Tsuge, K.; Tanaka, K. *Inorg. Chem.* **2001**, *40* (2), 329−337. (e) Fujihara, T.; Okamura, R.; Wada, T.; Tanaka, K. *Dalton Trans.* **2003**, No. 16, 3221−3226. (f) Hino, T.; Wada, T.; Fujihara, T.; Tanaka, K. *Chem. Lett.* **2004**, *33* (12), 1596−1597. (g) Okamura, R.; Wada, T.; Aikawa, K.; Nagata, T.; Tanaka, K. *Inorg. Chem.* **2004**, *43* (22), 7210−7217. (h) Wada, T.; Fujihara, T.; Tomori, M.; Ooyama, D.; Tanaka, K. *Bull. Chem. Soc. Jpn.* **2004**, *77* (4), 741−749. (i) Fujihara, T.; Okamura, R.; Tanaka, K. *Chem. Lett.* **2005**, *34* (11), 1562−1563 (j) Wada, T.; Tanaka, K. *Eur. J. Inorg. Chem.* **2005**, No. 19, 3832−3839.

(5) (a) Kobayashi, K.; Ohtsu, H.; Wada, T.; Tanaka, K. *Chem. Lett.* **2002**, No. 8, 868−869. (b) Kobayashi, K.; Ohtsu, H.; Wada, T.; Kato, T.; Tanaka, K. *J. Am. Chem. Soc.* **2003**, *125* (22), 6729−6739.

(6) Sullivan, B. P.; Calvert, J. M.; Meyer, T. J. *Inorg. Chem.* **1980**, *19* (5), 1404−7.

Scheme 3

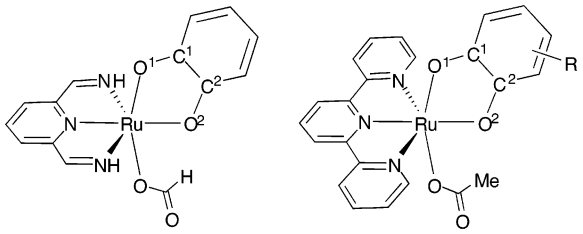

$C_{27}H_{26}N_3O_4Ru\cdot H_2O$: C, 56.34; H, 4.90; N, 7.30. Found: C, 56.06; H, 4.86; N, 7.25.

[Ru(OAc)(3,5-$Cl_2C_6H_2O_2$)(terpy)] (4). This complex was prepared in a manner similar to that of **2**. Yield: 54%. Anal. Calcd for $C_{23}H_{16}N_3O_4Cl_2Ru\cdot{}^1/_2H_2O$: C, 47.68; H, 2.96; N, 7.25. Found: C, 47.38; H, 2.96; N, 7.28.

Instruments. UV−vis−NIR spectra were recorded on a Shimazu UVPC-3100 UV−vis−NIR scanning spectrophotometer. ESI-MS spectra were measured with a Shimazu LCMS-2010 liquid chromatograph−mass spectrometer and a Waters-Micromass LCT. Elemental analyses were carried out at the Research Center for Molecular-Scale Nanoscience at the Institute for Molecular Science. Resonance Raman spectra were measured with a JASCO NRS-1000 laser Raman spectrometer. Cyclic voltammetry (CV) was performed with an ALS/Chi model 660 electrochemical analyzer. Cyclic voltammograms were recorded in CH_2Cl_2 containing 0.1 mol dm^{-3} *n*-Bu_4NClO_4 as an electrolyte at a scan rate of 50 mV s^{-1} at 298 K using a glassy carbon disk, a Pt wire, and Ag/Ag-(NO_3) (0.01 mol dm^{-3}) as working, counter, and reference electrodes, respectively. All potentials were converted to SCE ($E_{SCE} = E_{Ag/AgNO_3} + 0.330$ V).

Electronic Structure Calculations. The geometry, Kohn−Sham orbital (KO), and spin density distribution of **1**, **2**, **3**, and **5** were calculated with density functional methods. These ruthenium complexes were optimized under C_s symmetry by the ONIOM method, which has been proven to be a powerful tool for the theoretical treatment of large molecular systems.[8] We divided the real system of Ru(OAc) complexes into two layers as shown in Scheme 3. The small models of layer 1 (Scheme 3) were treated with the UB3LYP method[9] with the basis set denoted as 631SDD consisting of a Stuttgart effective core potential (SDD)[10] for the transition metals and the 6-31G(d) basis set[11] for the rest.

The fully real models of layer 2 (Scheme 3) were treated with the UB3LYP method with the basis set denoted as 321LAN consisting of an LANL2DZ effective core potential[12] for the transition metals and the 3-21G basis set for the rest.[11] Single-point energy calculations of the ONIOM-optimized structures were carried out at the UB3LYP/631SDD level for analysis of KOs and spin density distributions. All calculations were performed with the Gaussian 98 package.[13]

Results and Discussion

Electronic Structures of Ru(OAc) Complexes with Dioxolenes. A series of [Ru(OAc)(dioxolene)(terpy)] compounds were prepared and their physicochemical properties depending on the substituents on the dioxolene ligand were examined. The ruthenium complexes [Ru(OAc)(3,5-*t*-$Bu_2C_6H_2O_2$)(terpy)] (**1**), [Ru(OAc)(4-*t*-$BuC_6H_3O_2$)(terpy)] (**2**), [Ru(OAc)(4-$ClC_6H_3O_2$)(terpy)] (**3**), [Ru(OAc)(3,5-$Cl_2C_6H_2O_2$)(terpy)] (**4**), and [Ru(OAc)($Cl_4C_6O_2$)(terpy)] (**5**) were obtained by the reaction of $RuCl_3$(terpy) with 3 equiv of $AgBF_4$ followed by treatment with the corresponding catechols in the presence of an excess amount of AcOK in MeOH. Complexes **1**−**5** were isolated as neutral forms without counterions. The actual electronic structure of **1**−**5**, therefore, is either the Ru^{II}(sq) or the Ru^{III}(cat) form or lies somewhere between the two extreme resonance forms (eq 1).

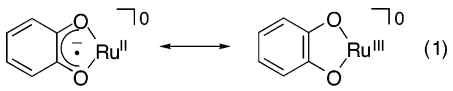

EPR spectroscopy in glassy frozen solutions is a powerful methodology to investigate the electronic structure of transition-metal dioxolene complexes,[3f,14] since the amount of spin on the metal is evaluated by the anisotropy of the **g** tensor as quantified by $\Delta g = g_1 - g_3$, and the isotropic *g* factor $\langle g \rangle$ reflects the deviation from the values for the free electron ($g = 2.0023$) and for free semiquinone anion radicals ($g =$ ca. 2.005).[14a] The EPR spectrum of a glassy frozen solution of **1** at 20 K exhibits an anisotropic signal with $g_1 = 2.104$, $g_2 = 2.042$, and $g_3 = 1.951$ (Figure 1a).

The anisotropy value $\Delta g = 0.153$ of **1** suggests more or less an involvement of the Ru^{III}(cat) (d^5 low-spin) contribution, since the value is slightly larger than that of $\Delta g = 0.082$ of $[Ru^{II}(sq)(bpy)_2]^{+}$ [3b] and much smaller than $\Delta g = 0.833$ and 1.00 of $[Ru^{III}(NH_3)_4(dpe)]$ (dpe = 2-(3,4-dihydroxyphenyl)ethanoato)[15] and $[Ru^{III}(acac)_3]$ (acac = acetylacetonato),[16] respectively, as typical Ru^{III} complexes (Table 1).

(7) Kurihara, M.; Daniele, S.; Tsuge, K.; Sugimoto, H.; Tanaka, K. *Bull. Chem. Soc. Jpn.* **1998**, *71* (4), 867−875.
(8) (a) Maseras, F.; Morokuma, K. *J. Comput. Chem.* **1995**, *16* (9), 1170−9. (b) Svensson, M.; Humbel, S.; Froese, R. D. J.; Matsubara, T.; Sieber, S.; Morokuma, K. *J. Phys. Chem.* **1996**, *100* (50), 19357−19363. (c) Dapprich, S.; Komiromi, I.; Byun, K. S.; Morokuma, K.; Frisch, M. J. *THEOCHEM* **1999**, *461*−*462*, 1−21. (d) Vreven, T.; Morokuma, K. *J. Comput. Chem.* **2000**, *21* (16), 1419−1432.
(9) (a) Becke, A. D. *J. Chem. Phys.* **1993**, *98* (7), 5648−52. (b) Lee, C.; Yang, W.; Parr, R. G. *Phys. Rev. B* **1988**, *37* (2), 785−9.
(10) Dolg, M.; Wedig, U.; Stoll, H.; Preuss, H. *J. Chem. Phys.* **1987**, *86* (2), 866−72.
(11) Hehre, W. J. R., L.; Schleyer, P. V. R.; Pople, J. A. *Ab initio Molecular Orbital Theory*; John Wiley: New York, 1986.
(12) Hay, P. J.; Wadt, W. R. *J. Chem. Phys.* **1985**, *82* (1), 299−310.
(13) Frisch, M. J. T., G. W.; Schlegel, H. B.; Scuseria, G. E.; Robb, M. A.; Cheeseman, J. R.; Zakrzewski, V. G.; Montgomery, J. A., Jr.; Stratmann, R. E.; Burant, J. C.; Dapprich, S.; Millam, J. M.; Daniels, A. D.; Kudin, K. N.; Strain, M. C.; Farkas, O.; Tomasi, J.; Barone, V.; Cossi, M.; Cammi, R.; Mennucci, B.; Pomelli, C.; Adamo, C.; Clifford, S.; Ochterski, J.; Petersson, G. A.; Ayala, P. Y.; Cui, Q.; Morokuma, K.; Salvador, P.; Dannenberg, J. J.; Malick, D. K.; Rabuck, A. D.; Raghavachari, K.; Foresman, J. B.; Cioslowski, J.; Ortiz, J. V.; Baboul, A. G.; Stefanov, B. B.; Liu, G.; Liashenko, A.; Piskorz, P.; Komaromi, I.; Gomperts, R.; Martin, R. L.; Fox, D. J.; Keith, T.; Al-Laham, M. A.; Peng, C. Y.; Nanayakkara, A.; Challacombe, M.; Gill, P. M. W.; Johnson, B.; Chen, W.; Wong, M. W.; Andres, J. L.; Gonzalez, C.; Head-Gordon, M.; Replogle, E. S.; Pople, J. A. *Gaussian 98*, Revision A.11; Gaussian, Inc.: Pittsburgh, PA, 2001.
(14) (a) Kaim, W. *Coord. Chem. Rev.* **1987**, *76*, 187−235. (b) Patra, S.; Sarkar, B.; Mobin, S. M.; Kaim, W.; Lahiri, G. K. *Inorg. Chem.* **2003**, *42* (20), 6469−6473. (c) Ye, S.; Sarkar, B.; Duboc, C.; Fiedler, J.; Kaim, W. *Inorg. Chem.* **2005**, *44* (8), 2843−2847.
(15) Salmonsen, R. B.; Abelleira, A.; Clarke, M. J. *Inorg. Chem.* **1984**, *23*, 387.
(16) DeSimone, R. E. *J. Am. Chem. Soc.* **1973**, *95* (19), 6238−44.

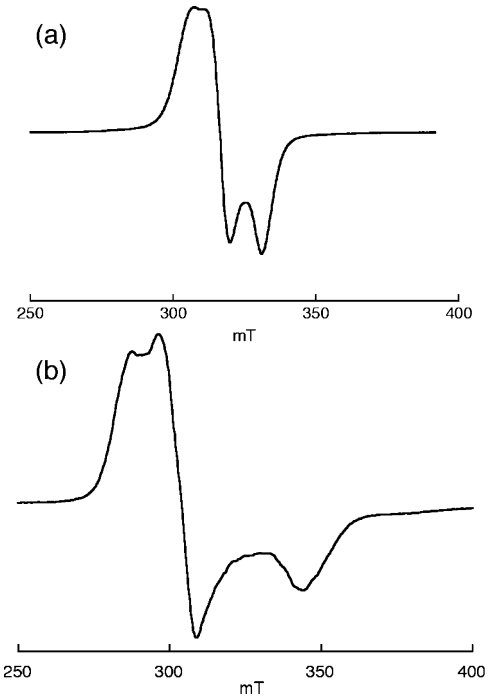

Figure 1. EPR spectra of **1** (a) and **3** (b) in glassy CH_2Cl_2/MeOH (95:5) at 20 K (microwave frequency, 9.029006 GHz; microwave power, 0.9980 mW; modulation width, 1.0 mT; modulation amplitude, 16 mT).

Table 1. EPR Data of **1**−**5** in CH_2Cl_2/MeOH (95:5, v/v) at 20 K

complex	g_1	g_2	g_3	Δg^a	$\langle g \rangle^b$
1[c]	2.104	2.042	1.951	0.153	2.033
2[c]	2.175	2.086	1.910	0.265	2.048
3[c]	2.229	2.116	1.871	0.358	2.077
4[c]	2.226	2.121	1.862	0.364	2.075
5[c]	2.242	2.097	1.846	0.396	2.068
$[Ru^{III}(NH_3)_4(dpe)]$[15]	2.722	2.722	1.889	0.833	2.476
$[Ru^{II}(t\text{-}Bu_2sq)(bpy)_2]^{+}$ [3b]	2.067	1.985	1.985	0.082	2.013
$[Ru^{III}(acac)_3]$[16]	2.45	2.16	1.45	1.00	2.06

[a] $\Delta g = g_1 - g_3$. [b] $\langle g \rangle = [(g_1^2 + g_2^2 + g_3^2)/3]^{1/2}$. [c] Microwave frequency, 9.029006 GHz; microwave power, 0.9980 mW; modulation width, 1.0 mT; modulation amplitude, 16 mT.

The isotropic g value $\langle g \rangle = [(g_1^2 + g_2^2 + g_3^2)/3]^{1/2} = 2.033$ of **1** is the lowest among the present complexes but is still relatively larger than 2.005 for free semiquinone. The Δg value increases in the order **1** < **2** < **3** < **4** < **5**, and the isotropic g value also has the same tendency. In addition, complexes **1**, **2**, and **3** exhibited an EPR signal in CH_2Cl_2 at room temperature, whereas **4** and **5** did not show any signals under the same conditions. Such a difference may result from the shift of the resonance of eq 1 to the left (ligand-based spin in **1**−**3**) and to the right (metal-based spin in **4** and **5**), because localization of spin on a metal would lead to rapid relaxation and display a broad signal with large anisotropy.[17] The electronic structure of **1**, therefore, is the closest to that of Ru^{II}(sq) among the present complexes, and the Ru^{III}(cat) character gradually increases with increasing electron-withdrawing ability of the substituents on the dioxolene ligand.

(17) (a) Medhi, O. K.; Agarwala, U. *Inorg. Chem.* **1980**, *19* (5), 1381−4. (b) Sakaki, S.; Yanase, Y.; Hagiwara, N.; Takeshita, T.; Naganuma, H.; Ohyoshi, A.; Ohkubo, K. *J. Phys. Chem.* **1982**, *86* (6), 1038−43.

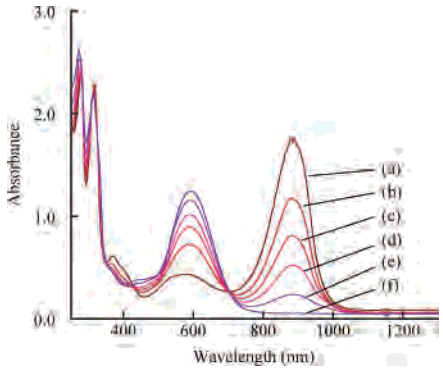

Figure 2. Electronic absorption spectra of **1** in the presence of various amounts (equiv) of $Ce(NH_4)_2(NO_3)_6$ in CH_2Cl_2: 0 (a), 0.2 (b), 0.4 (c), 0.6 (d), 0.8 (e), and 1.0 (f).

Table 2. CT Bands and Redox Potentials of **1**−**5** in CH_2Cl_2

complex	λ_{max}/nm (ϵ/$M^{-1}cm^{-1}$)	potential[a]/ V vs SCE	
1	883 (18600)	−0.68	+0.18
2	897 (15300)	−0.57	+0.27
3	890 (15200)	−0.45	+0.44
4	885 (14100)	−0.37	+0.57
5	884 (11700)	−0.28	+0.67

[a] Cyclic voltammograms were recorded in CH_2Cl_2 containing n-Bu_4NClO_4 (0.1 mol dm^{-3}) as an electrolyte at a scan rate of 50 mV s^{-1}at 298 K using a glassy carbon disk, a Pt wire, and Ag/$Ag(NO_3)$ (0.01 mol dm^{-3}) as working, counter, and reference electrodes, respectively. All potentials were converted to SCE ($E_{SCE} = E_{Ag/AgNO_3} + 0.330$ V).

In contrast to the EPR spectra, the electronic absorption spectra of **1**−**5** are very close to each other except for the absorption coefficients (Figure 2 and Table 2).

Complex **1** shows strong electronic absorption bands at 278, 316, 367, 403, 537, 592, and 883 nm (Figure 2a). The patterns and the positions of the 278, 316, 367, and 592 nm bands of **1** are close to those of $[Ru^{II}(Cl)(acac)(terpy)]$ (278, 318, 386, and 610 nm).[18] The remaining 883 nm band of **1**, therefore, is associated with the charge-transfer transition within the Ru−dioxolene framework from the analogy to the strong band at 850 nm of $[Ru^{II}(t\text{-}Bu_2sq)(bpy)_2]^{+}$, which is assigned as the MLCT band by Lever and co-workers. [12] The charge-transfer transition band at 883 nm could be related to the bonding π-orbital (dπ(Ru) + π*(sq)), singly occupied molecular orbital (SOMO)) and antibonding π*-orbital (dπ(Ru) − π*(sq), lowest unoccupied molecular orbital (LUMO)). The intensity of the band would reflect the degree of orbital overlapping between dπ(Ru) and π*-(sq) in the ground and excited states.[2] A decrease in the absorption coefficient of the band around $\lambda_{max} = 850$ nm in the order **1** > **2** > **3** > **4** > **5**, therefore, may result from a successive decrease of orbital mixings between dπ(Ru) and π*(sq) of the complexes.

The cyclic voltammograms of **1**−**5** show two reversible redox couples in the range from +1.0 to −1.0 V in CH_2Cl_2 (vs SCE; Figure 3 and Table 2). The rest potentials of the complexes are located between the two redox potentials, indicating that all the complexes undergo reversible one-electron oxidation and reduction reactions in the potential

(18) Adeyemi, S. A.; Dovletoglou, A.; Guadalupe, A. R.; Meyer, T. J. *Inorg. Chem.* **1992**, *31* (8), 1375−83.

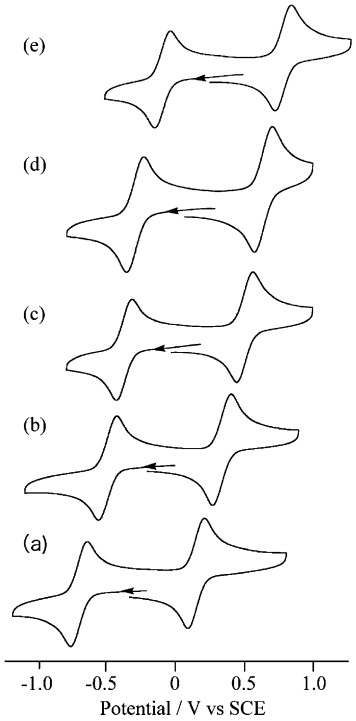

Figure 3. Cyclic voltammograms of **1** (a), **2** (b), **3** (c), **4** (d), and **5** (e) in the presence of n-Bu_4NClO_4 (0.1 mol dm^{-3}) in CH_2Cl_2. A glassy carbon disk, a Pt wire, and $Ag/Ag(NO_3)$ (0.01 mol dm^{-3}) as working, counter, and reference electrodes, respectively, were used with a sweep rate of 50 mV s^{-1} at 298 K. Potential scanning started from the rest potentials of the complex solutions. All potentials were converted to SCE ($E_{SCE} = E_{Ag/AgNO_3} + 0.330$ V).

range. As expected from the substituent effects, the redox potentials of $E_{1/2}(1)$ (positive side) and $E_{1/2}(2)$ (negative side) shift to more positive potentials in the order **1** < **2** < **3** < **4** < **5**, which followed the Hammett σ rule (see Figure S1 in the Supporting Information). The one-electron-reduced forms of **1**−**5** definitely have the Ru^{II}(cat) framework, which does not exhibit the CT transition because the occupied dπ- and pπ-orbitals of Ru^{II} and cat, respectively. On the other hand, one-electron-oxidized forms of **1**−**5** display strong CT bands. Figure 2 shows the electronic absorption spectra of a CH_2Cl_2 solution of **1** in the presence of various amount of $Ce^{IV}(NH_4)_2(NO_3)_6$ as a one-electron oxidant. The absorbance of the 883 nm band of **1** gradually decreased with an increase of the amount of Ce^{IV} and completely disappeared in the presence of 1.0 equiv of the oxidant. Instead, a new band emerged at 592 nm assigned to the CT band resulting from the Ru−dioxolene chromophore of $\mathbf{1}^+$ (vide infra). Taking advantage of the appearance of the strong absorption band at 592 nm of $\mathbf{1}^+$, resonance Raman spectra of the cationic complex were measured under illumination of 632.8 nm excitation light. Three bands at 565, 593, and 1356 cm^{-1}, which were strongly enhanced in intensity under the experimental conditions, were reasonably associated with the stretching modes relevant to the Ru−dioxolene framework (Figure 4).

The 565 and 593 cm^{-1} bands are tentatively assigned to the ν(Ru−O) mode coupled with the ν(C−C) and ring deformation modes on the basis of the resonance Raman spectra of the one-electron oxidation form of [Ru(3,5-t-Bu_2-sq)(bpy)$_2$]$^+$.[3e] The remaining 1356 nm band of $\mathbf{1}^+$ probably results from the C−O stretching mode of the dioxolene ligand. The ν(CO) bands of the M(cat), M(sq), and M(q) complexes generally appear in ranges of 1250−1275, 1400−1500, and 1630−1640 cm^{-1}, respectively.[2c] According to the criteria, the ν(CO) band of $\mathbf{1}^+$ seems to be an intermediate between those of the M(cat) and M(sq) forms as reported in the electronic structures of some Ru−dioxolene and Os−dioxolene complexes.[2,3] However, a small difference in the ν(CO) band between **1** (IR in KBr: 1360 cm^{-1}) and $\mathbf{1}^+$ (1356 cm^{-1}) strongly suggests that **1** undergoes metal-centered oxidation rather than ligand-centered oxidation. The ν(CO) bands of **1** and $\mathbf{1}^+$, therefore, may be interpreted as metal-centered oxidation of the Ru^{II}(sq) framework, affording the Ru^{III}(sq) framework. Attempts to measure the resonance Raman spectra of the one-electron-oxidized forms of **2**−**5**, however, were unsuccessful due to extreme lability of these cationic complexes under illumination of the 632.8 nm excitation light.

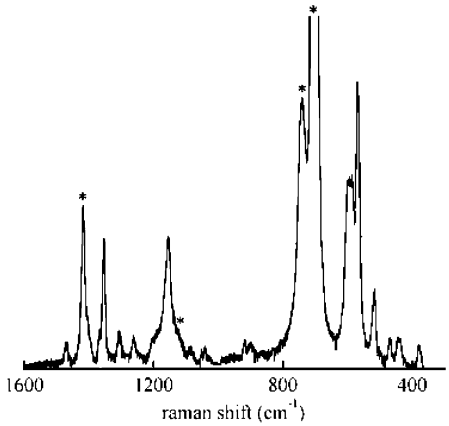

Figure 4. Resonance Raman spectrum of $\mathbf{1}^+$ in CH_2Cl_2 at room temperature, 632.8 nm excitation. Asterisks indicate solvent signals.

Table 3. Relevant Structural Parameters of **1**−**5** Optimized at the ONIOM(UB3LYP/631SDD:UB3LYP/321LAN) Level

complex	Ru−O[1]/ Å	Ru−O[2]/ Å	Ru−OAc/ Å	O[1]−C[3]/ Å	O[2]−C[4]/ Å	Ru−N[5]/ Å	Ru−N[6]/ Å
1	2.063	2.095	2.057	1.310	1.311	2.078	1.942
1 (exptl)	2.030	2.019	2.062	1.328	1.324	2.053	1.952
2	2.068	2.096	2.054	1.309	1.306	2.076	1.943
3	2.065	2.091	2.053	1.309	1.307	2.053	1.946
5	2.049	2.087	2.046	1.308	1.302	2.079	1.951

Table 4. Spin Density Distribution and Natural Population Analysis in **1**−**5** Optimized at the ONIOM(UB3LYP/631SDD:UB3LYP/321LAN) Level

	spin density				natural charge			
complex	Ru	dioxolene	OAc	terpy	Ru	dioxolene	OAc	terpy
1	0.244	0.783	0.003	−0.030	0.830	−0.663	−0.623	0.456
2	0.250	0.777	0.003	−0.010	0.830	−0.668	−0.620	0.458
3	0.304	0.722	0.004	−0.030	0.841	−0.722	−0.616	0.496
5	0.408	0.612	0.009	−0.029	0.873	−0.836	−0.603	0.566

DFT Studies. Geometry optimization of **1**−**3** and **5** was performed at the ONIOM(UB3lYP/631SDD:UB3LYP/321LAN) level. All complexes show C_s symmetry with the Ru−O[1] bond oriented along the z axis. Three nitrogen atoms of terpy and one oxygen of dioxolene are bonded to Ru in the equatorial plane, and the remaining two oxygens of the

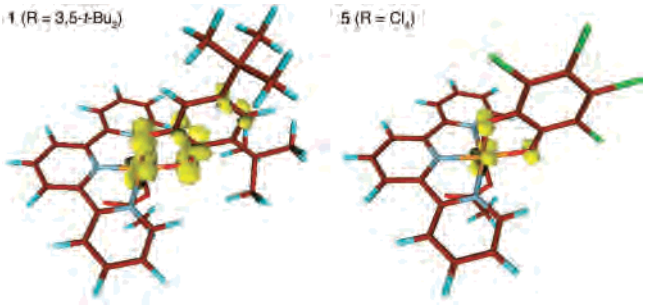

Figure 5. Spin density surface plots (spin density contour 0.05) of **1** and **5** optimized with UB3LYP/631SDD level calculations of ONIOM-optimized structures.

dioxolene and acetate ligands are linked to the central metal in the axial position (see Figure S3 in the Supporting Information). The relevant structural parameters of ONIOM-optimized geometries are listed in Table 3.

The metal−ligand bond lengths in the optimized structure are comparable to those of the crystal structure of **1**.[5b] The Ru−O^1 and Ru−O^2 lengths tend to be longer than those of the experimental values (Ru−O^1, +0.033 Å, +1.6%; Ru−O^2, +0.076 Å, +3.6%), whereas the Ru−OAc length is slightly shorter (−0.005 Å, −0.2%). With an increase of the number of electron-withdrawing substituents (e.g., Cl) on the dioxolene ligand, both the Ru−O^1 and Ru−O^2 lengths become shorter (the difference in the Ru−O^1 and Ru−O^2 bond lengths is up to 0.019 Å), whereas the O^1−C^3 and O^2−C^4 bond lengths change by less than 0.01 Å. Detailed analyses of the C−O bond lengths of the dioxolene ligands have been documentated;[19] those for semiquinonates and catecholates are in the ranges 1.27−1.31 and 1.34−1.47 Å, respectively. The calculated C^3−O^1 and C^4−O^2 bond lengths of **1**−**5** converge on ca. 1.31 (±0.018 Å). However, these

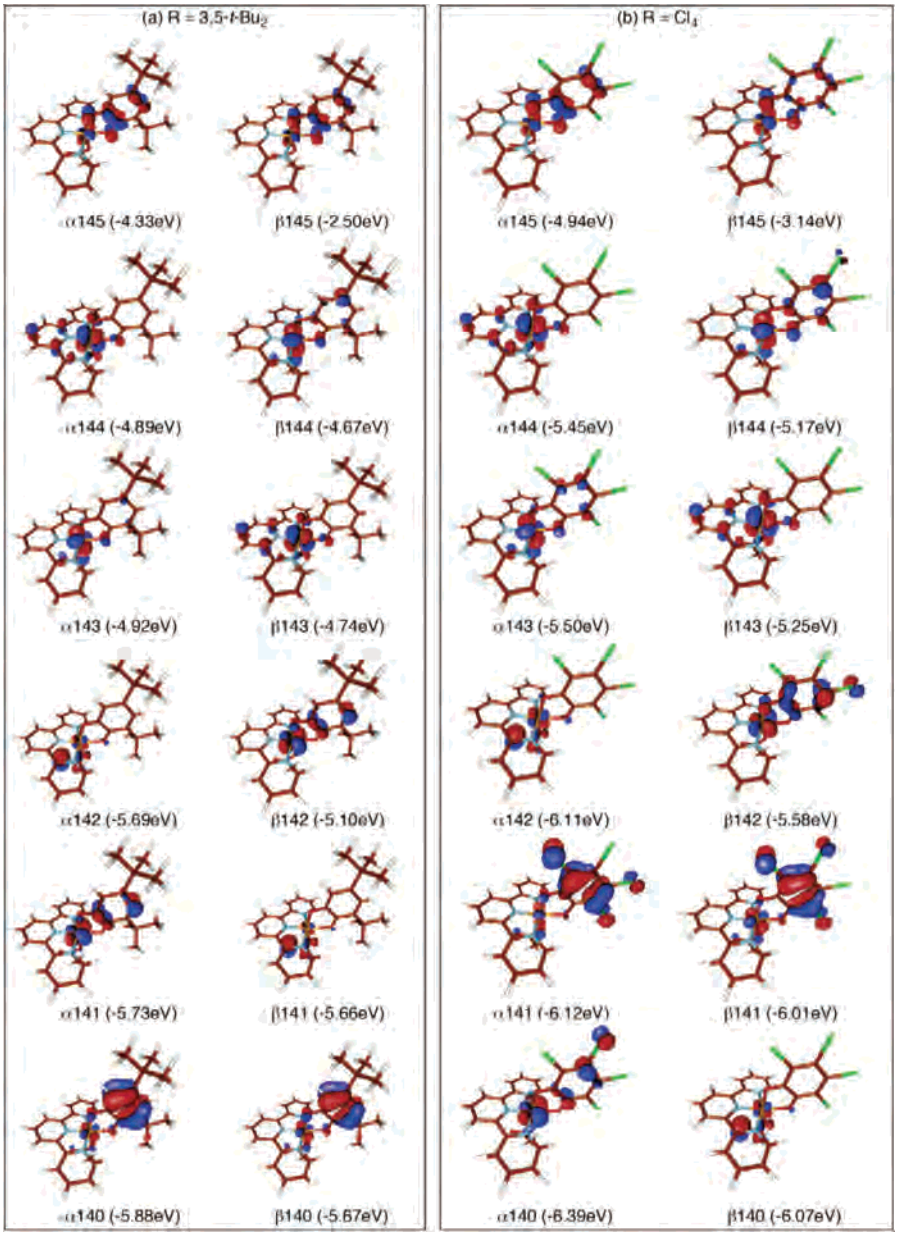

Figure 6. Kohn−Sham orbitals (orbital contour 0.05) of complexes (a) **1** and (b) **5** optimized with UB3LYP/631SDD level calculations of ONIOM-optimized structures.

Scheme 4

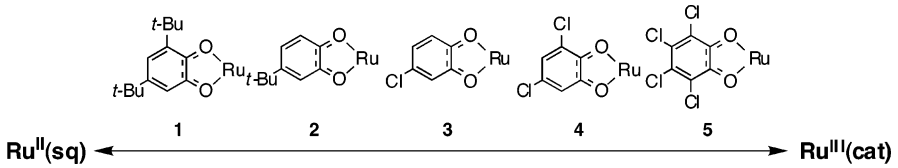

structural parameters do not necessarily imply that all the complexes have Ru^{II}(sq) structures by considering the disagreement (or error) of the C−O bond lengths of **1** determined by X-ray analysis and optimized by the unrestricted DFT calculation (Table 3).

Spin density distributions and KOs in the frontier region were analyzed in detail. Mulliken atomic spin densities reveal consecutive changes of the electronic structure of **1**−**3** and **5**, depending on the substituents on dioxolene. As summarized in Table 4, the spin densities are mostly located on Ru and the dioxolene ligands. The Ru spin density increases with an increase of the number of electron-withdrawing substituents on the dioxolene ligand. The largest spin density on Ru was observed in the case of **5** (0.408), whereas the smallest one was **1** (0.244). In contrast, the dioxolene spin density decreases with an increase of Cl-substituted groups on the dioxolene ligand. These results indicate that the electron-withdrawing substituent on the dioxolene ligand emphasizes a description of Ru^{III}(cat) over Ru^{II}(sq). Thus, chloride on dioxolene shifts the electron density into the dioxolene moiety and increases the Ru^{III}(cat) contribution to the complexes, as shown by the EPR spectra of the complexes. It is also worth noting that the OAc spin density grows up in the case of **5**. This may correlate with formation of the stable $[Ru(O^{\bullet}H)(4\text{-}ClC_6H_3O_2)(terpy)]^+$, which is generated by deprotonation of $[Ru(OH_2)(4\text{-}ClC_6H_3O_2)(terpy)]^{2+}$ followed by intramolecular electron transfer from OH^- to the $[Ru(4\text{-}ClC_6H_3O_2)]$ moiety.

Contour plots of **1** and **5** clearly demonstrate variation of the spin density distribution depending on the substituents on dioxolene (Figure 5). In complex **1**, the spin density was delocalized over the Ru−dioxolene moiety, whereas it was localized on Ru, O^1, and O^2 in **5**. The spin density, i.e., the sum of unpaired α and β electrons, is interpreted as the difference between the α and β spin density contributions to the total electron density. In addition to the unpaired electron in the SOMO, spin polarization would also largely contribute the spin density because the unpaired electron polarizes the electron spins in doubly occupied orbitals with the consequence that the α and β spin−orbitals adopt different spatial distributions. As a result, the spin density is not necessarily the same as the unpaired electron density in the SOMO.[20] A closer look at the description of the α and β spin KOs of **1** and **5** reveals the difference in the spin density of the two complexes (Figure 6).

The spin density distribution of **1** is delocalized between Ru and the dioxolene moiety in a manner similar to that of the SOMO (α145 in Figure 6a). The KOs of the α spin electron of **1** almost parallel those of the β spin electron (Figure 6a). As a consequence, the spin density distribution of **1** arises mostly from the SOMO spin density. On the other hand, the spin density distribution of **5** is relatively localized on Ru, O^1, and O^2. Furthermore, the KOs of α and β spin electrons show patterns much different from each other (Figure 6b). This indicates that spin polarization largely contributes to the spin density distribution of **5** and causes much more spin localization on Ru, O^1, and O^2 than that of **1**. As a result of the increasing spin polarization contribution in **5**, the largest spin density on Ru amplified the Ru^{III}(cat) character in **5**, even appearing identical in two SOMO pictures of **1** and **5** (α145 in Figure 6). Thus, detailed analysis of the KOs of **1** and **5** demonstrates that spin polarization induced by the electron-withdrawing group on the dioxolene ligand significantly influences the electronic structure of the Ru−dioxolene complex. In addition, the electron-withdrawing group shifts the energies of the SOMO and LUMO levels in complexes **1**−**3** and **5** to more negative energies (Table 5). This is comparable to the shift of the redox waves of the complexes toward more positive potential in the cyclic voltammograms with an increase of the number of electron-withdrawing substituents on the dioxolene ligand as mentioned above.

Table 5. Energy Levels (eV) of Both the SOMO and LUMO in **1**−**5** Optimized at the ONIOM(UB3LYP/631SDD:UB3LYP/321LAN) Level

	1	**2**	**3**	**5**
LUMO	−2.5 (β145)	−2.5 (β129)	−2.8 (β121)	−3.1 (β145)
SOMO	−4.3 (α145)	−4.3 (α129)	−4.6 (α121)	−4.9 (α145)

Together with the spin density and KO analysis described above, natural population analysis provided trends of intramolecular electron transfer in detail (Table 4). In the case of **1**, 0.830 and −0.663 charges are distributed to Ru and dioxolene, respectively. The proportion of the charge distribution of the Ru−dioxolene moiety is correlated with the substituents on dioxolene. The positive charge on Ru and the negative charge on dioxolene increase with an increase of the electron-withdrawing substituents on dioxolene. In particular, the most positive charge (0.873) on Ru and negative charge (−0.836) on the dioxolene moiety were obtained in **5**. The dioxolene ligand substituted with chloride, therefore, draws the d-electron on Ru into the dioxolene moiety. As a result, the Ru^{III}(cat) character is remarkably enhanced in the case of **5**.

Conclusion

EPR, electrochemistry, and DFT calculations clearly demonstrated successive changes of the electronic structure of the Ru−dioxolene framework of **1**−**5** depending on the

(19) Carugo, O.; Castellani, C. B.; Djinovic, K.; Rizzi, M. *J. Chem. Soc., Dalton Trans.* **1992**, 837.
(20) See, e.g.: (a) Braden, D. A.; Tyler, D. R. *Organometallics* **1998**, *17*, 4060−4064. (b) Remenyi, C.; Kaupp, M. *J. Am. Chem. Soc.* **2005**, *127*, 11399−11413 and references therein.

substituents of the dioxolene ligands. The electronic states of these complexes formally lie somewhere between those of Ru^{II}(sq) and Ru^{III}(cat). The contribution of Ru^{III}(cat) continuously increases with an increase of the electron-withdrawing substituents on the dioxolene ligands, as depicted in Scheme 4.

Supporting Information Available: Hammett plots of redox potentials of complexes **1**−**5** and corresponding free quinones and optimized structures of complexes **1**−**3** and **5**. This material is available free of charge via the Internet at http://pubs.acs.org.

IC060696I